Dalton Transactions

Accepted Manuscript

ROYAL SOCIETY OF CHEMISTRY

www.rsc.org/dalton

Abnormal luminescent property of Mn^{2+} in α-$LiZnBO_3$:Mn^{2+}

Hongrun Wang[a], Li Wu[b]*, Huan Yi[b], Biao Wang[a], Liwei Wu[b], Yuelong Gu[a], Yi Zhang[a]*

a Institute of Photo-electronic Thin Film Devices and Technology and Tianjin Key Laboratory of Photo-electronic Thin Film Devices and Technology, Nankai University, Tianjin 300071, China. Email: yizhang@nankai.edu.cn; Tel: +86-22-23508572-8018, Fax: +86-22-23508912

b The MOE key laboratory of weak-Light Nonlinear Photonics, School of Physics, Nankai University, Tianjin 300071. Email: lwu@nankai.edu.cn; Tel: +86-22-23506257, Fax: +86-22-23505409

Abstract

Mn^{2+}-activated red phosphor α-$LiZnBO_3$:Mn^{2+} was synthesized by solid state reaction. ESR spectra prove that the doped ions are Mn^{2+}. The doped Mn^{2+} ion is inclined to occupy Zn^{2+} site which is tetrahedral coordination. The diffuse reflection spectra indicate that α-$LiZnBO_3$:Mn^{2+} has strong absorption in the range of 400-450nm. Excited at 431 nm, abnormal red emission band in the wavelength of 550-800nm is observed, which is because the strong crystal field induced by distorted tetrahedral. The emission bands are centered at 647 nm, regardless of the excitation wavelength and Mn^{2+} doping concentration. The temperature-dependent PL results reveal that α-$LiZnBO_3$:Mn^{2+} is thermal stable but the emission peak moves to shorter wavelength as temperature increase because of the decrease of the crystal field.

Introduction

Transition metal Mn^{2+} has $3d^5$ configuration and shows a broad emission band, which is an desirable luminescence center in many phosphors used for several fields, such as fluorescent lamps, cathode ray tubes (CRTs), plasma display panels (PDPs), and white light-emitting diodes (W-LEDs). To search for phosphors doped by Mn^{2+} used in lighting and displays, lots of Zn-based compounds have been investigated， such as $Zn_2SiO_4:Mn^{2+}$,[1] $ZnGa_2O_4:Mn^{2+}$,[2] $Ba_2ZnS_3:Mn^{2+}$,[3] $LiZnPO_4:Mn^{2+}$.[4] All these compounds contain similar structural blocks, which is $[ZnX_4]$ (X=O, S and Se). In these compounds, Mn^{2+} ions are expected to substitute Zn^{2+} ions because of similar ionic radius and charge (the radius of Mn^{2+} is 0.66 Å when coordination number CN=4 and radius of Zn^{2+} is 0.60 Å when CN=4). The position of the lowest excited state of Mn^{2+} strongly depends on the crystal field strength, which allows shifting the Mn^{2+} emission from green to red, depending on the crystal field strength of the substituted sites. Normally, tetrahedral coordinated Mn^{2+} (weak crystal field) usually gives a green emission while octahedral coordinated Mn^{2+} (strong crystal field) gives orange to red emission.[5] It is accepted that the emission intensity of Mn^{2+} is weak because the d-d transition of Mn^{2+} is spin and parity forbidden. However, recent studies indicate that tetrahedral coordinated Mn^{2+} can emit red light in some Zn-based compounds, such as $MZnOS:Mn^{2+}$ (M=Ca, Ba)[6] and β-$Zn_3B_2O_6:Mn^{2+}$.[7] This abnormal phenomenon is attracting increasing attention as it is important to understand the luminescent property of Mn^{2+} in specific host structure. In addition, compared with rare earth ions activated phosphors, Mn^{2+}-activated phosphors are inexpensive, which make it favorable in practical application.

Borates exhibit many excellent properties as host structure of phosphor because of their large band gap, excellent chemical and physical stability and low synthesizing temperature.[8] A variety of borates phosphors doped with rare earth ions and transitional metal ions have been reported, showing excellent luminescent property. [9-12] In the ternary system of Li_2O-ZnO-B_2O_3, two $LiZnBO_3$ polymorphs have been found: one by solid state reaction (α-$LiZnBO_3$) and another one is obtained by hydrothermal synthesis (β-$LiZnBO_3$). α-$LiZnBO_3$ was first reported by Lehman and Shadow.[13] The crystal structure of α-$LiZnBO_3$ is composed of ZnO_4 tetrahedra and BO_3 triangles by sharing O vertices and offer three-dimensional open channels for lithium ions .[14] In this structure, two inversion-center related ZnO_4 tetrahedra are linked by sharing one edge to form a Zn_2O_6 dimer. β-$LiZnBO_3$, on the other hand, is composed of ZnO_5 bi-pyramids and BO_3 groups. As introduced above, α-$LiZnBO_3$ can afford a proper crystal field environment for Mn^{2+} ions because it contains tetrahedral ZnO_4. If Mn^{2+} occupy Zn site inα-$LiZnBO_3$ host, green light will emit. In our work, however, red emission with high intensity was observed, which is very rare as the Mn^{2+} is obviously tetrahedral coordinated. In this paper, we discuss the abnormal luminescence properties of Mn^{2+} as well as the stability of Mn^{2+} activated α-$LiZnBO_3$.

Experimental

Synthesis of α-$LiZnBO_3$:xMn^{2+}

Mn^{2+} doped α-$LiZnBO_3$ was synthesized by traditional high temperature solid state reaction method. The starting materials were analytical Li_2CO_3, ZnO, H_3BO_3, and $MnCO_3$. The weighed raw materials were mixed homogeneously in an agate mortar and then sintered at 500 ^oC for 24 h. Then the presintered sample was reground and

transferred to alumina boat and heated at 900 ^{o}C under a reducing atmosphere (15%H_2/85%Ar) for 6h. The samples were cooled down to room temperature in the furnace, reground and pulverized for further measurements.

Characterizations

The phase identification of as-prepared powders was checked at room temperature by a PANalytical X'Pert Pro powder X-ray diffractometer with Cu-Kα radiation (40 kV, 40 mA). The morphologies of the samples were measured by a scanning electron microscope(LEO1530VP, Zeiss). The crystal structure of α-$LiZnBO_3$ was draw by Crystal maker (version 2.2.4). Photoluminescence emission and excitation spectra and decay curve of the phosphors were measured by a FLS920 Fluorescence Spectrometer (Edinburgh Instruments) equipped with a Xe light source and double excitation monochromators. Diffuse reflectance spectra of the phosphors were measured by a UV-visible spectrophotometer (Hitachi U-4100) using the white $BaSO_4$ powder as a reference standard. The X-band (9.834GHz) ESR measurements of powder samples were carried out at room temperature using BRUKER EMX-6/1 EPR spectrometer of 100 kHz field modulation (2.002mW). The temperature-dependent luminescence properties were measured on a fluorescence spectrophotometer (F-4600, HITACHI, Japan) with a photomultiplier tube operating at 400 V, and a 150 W Xe lamp used as the excitation lamp. The internal quantum efficiency of optimized-composition phosphor α-$LiZnBO_3$:0.07Mn^{2+} was determined on an FLS920 spectrometer under excitation of 431 nm.

Results and discussion

Crystal structure and morphology of α-$LiZnBO_3$:Mn^{2+}

Room temperature XRD patterns of α-$LiZnBO_3$:xMn^{2+}(x=0.05-0.11) as well as standard card of α-$LiZnBO_3$ is shown in Fig.1(a). All XRD patterns of α-$LiZnBO_3$:xMn^{2+}(x=0.05-0.11) is found similar to each other and agree with that of α-$LiZnBO_3$ (PCPDF#-049-0530). This indicates that the doped Mn^{2+} ions do not induce significant changes in crystal structure of α-$LiZnBO_3$. A trace amount of $LiBO_2$ phase exists in the as-synthesized phosphors though the samples sintered several time at high temperature.

The XRD data demonstrate that the title host crystallizes with the monoclinic structure with parameter lattices a=8.746(2) Å, b=5.091(1) Å, c=6.129(1) Å, β=118.75(3)° and space group of C2/c. Fig. 1(b) shows the crystal structure of α-$LiZnBO_3$. It consists of vertex-sharing ZnO_4 tetrahedra, BO_3 triangles, and five-fold coordinated Li by O. Each Zn atom is coordinated by four O atoms and forms a distorted tetrahedral configuration, and two inversion-center ZnO_4 tetrahedra are linked by sharing one edge to form a Zn_2O_6 dimer.[14] The radius of Zn^{2+} is 0.60 Å as CN is 4, which is very close to the radius of Mn^{2+} (0.66 Å as CN=4). Considering the charge balance as well as the crystal environment afforded to Mn^{2+}, the doped Mn^{2+} is expected to occupy Zn^{2+}, which will be confirmed by the later results.

The morphology of the α-$LiZnBO_3$:0.07Mn^{2+} sample prepared by solid state reaction is shown in Fig. 2. The α-$LiZnBO_3$:0.07Mn^{2+} sample consists of aggregated particles with size ranging from 8-18 μm. The larger particles are attributed to the Li content in the $LiZnBO_3$ host, which enhances grain growth and improves crystallinity.[15]

ESR study of α-LiZnBO$_3$:Mn^{2+}

The room temperature powder ESR spectra (dI/dH) of the undoped and diluted doped α-LiZnBO$_3$:xMn^{2+} (x=0.001, 0.01, 0.02, 0.04) are shown in Fig. 3. Obviously, there is no resonance peak exist in the undoped α-LiZnBO$_3$, which indicates that the undoped sample does not contain any unpaired electron. However, as Mn^{2+} doped into α-LiZnBO$_3$, strong and broad resonance peaks exist, showing the contribution of Mn^{2+} spin. These spectra contain resonance absorptions centered at g ≈ 2.0 and g ≈ 4.21 factors. The g value around 2.0 shows the characteristic of an extended exchange coupled Mn^{2+} system. The resonance absorption line detected at g ≈ 2.0 is assigned to manganese ions disposed in the weak crystal field, while resonance absorption line occurring at g ≈ 4.21 is because of the Mn^{2+} ions disposed in strong crystal field.[16-17] As shown in the inset in the Fig. 3, the resonance from the sample doped by 0.1 at.% Mn^{2+} is composed of six well-defined hyperfine structure because of electron-nuclear (nuclear spin quantum number I=5/2 for ^{55}Mn nuclei) interaction. It can be also observed that there are many very small peaks (not shown here) in the magnetic field ranging from 3000 to 4000 Gauss for the sample of α-LiZnBO$_3$:0.01Mn^{2+}. As the Mn^{2+} content is increased, the resolution of the spectra is decreased and narrower lines cannot be observed.

Diffuse reflection spectra of undoped and Mn^{2+}doped α-LiZnBO$_3$

Fig. 4 shows the diffuse reflection spectra of undoped and Mn^{2+} doped α-LiZnBO$_3$ samples. In order to better understand the absorption of undoped and doped samples, the absorption spectra of undoped and Mn^{2+} doped α-LiZnBO$_3$ samples are calculated by the Kubelka-Munk function:[18]

$$F(R) = (1-R)^2 / 2R = K / S \quad (1)$$

where R, K and S refer to reflection, absorption and scattering coefficient, respectively. The absorption spectra are displayed in the inset of Fig. 4. The absorption in the region blow 220 nm is the ultraviolet absorption of host. The peak centered at 238 nm is ascribed to the charge transfer state (CTS) of O^{2-}–Mn^{2+} transition. The absorption in the region of 300-600 nm is mainly from d-d transition of Mn^{2+}.[6] The undoped sample shows a white daylight color because of strong reflection in visible region. For the Mn^{2+} doped α-$LiZnBO_3$ samples show white to pale pink color with Mn^{2+} concentration increasing. This is because of intensive absorption band in the range of 300-600nm, which can be attributed to the transition from the ground state $^6A_1$ of Mn^{2+} to its excited state. Besides, narrow strong absorption bands, which are situated in 400-450 nm, can be seen for all Mn^{2+} doped samples. Due to the absence of them in undoped sample, we think it is caused by the absorption of Mn^{2+} itself. Since every excited level of d^5 is either a spin quartet or a doublet, all transition from the ground sextet to them are spin-forbidden, and optical absorption of Mn^{2+} is usually weak, as in Zn_2SiO_4.[1] For the case of α-$LiZnBO_3$:Mn^{2+}, however, the absorption band is strong, indicating the selection rules should have been relaxed to some extent. Because Zn^{2+} is four coordinated by O^{2-} and formed a distorted tetrahedral. When Mn^{2+} ions occupy Zn^{2+}, a strong crystal field environment is afforded, as indicated by ESR results. As is discussed above, the tetrahedral Mn^{2+} occupy is distorted, resulting in strong crystal field, as in the case of CaZnOS.[6] Thus the selection is relaxed to some extent, and strong absorption is therefore observed.

Photoluminescence properties of α-$LiZnBO_3$:Mn^{2+}

Fig. 5 shows the room temperature PLE and PL spectra of α-$LiZnBO_3$:xMn^{2+} (x=0.07). Monitored at 647 nm, the excitation spectra show a broad band ranging from 230 to 280 nm and several narrow bands, which can be ascribed to CTS and Mn^{2+} d-d transitions, respectively. The CTS band originates from the transformation of electron on $2p^6$ orbit of O^{2-} to $3d^5$ orbit of Mn^{2+}. According to Orgel's diagram,[19] narrow band peaked at 327 nm comes from $^6A_1$-$^4E(^4D)$ transition. The excitation band ranging from 350 to 390 nm is from $^6A_1$-$^4T_2(D)$ transition. The emission band centered at 422nm, 431nm, 453nm correspond to $^6A_1$-$^4A_1$, $^4E(^4G)$, $^6A_1$-$^4T_2(^4G)$, and $^6A_1$-$^4T_1(^4G)$ transition of Mn^{2+} incorporated in α-$LiZnBO_3$, respectively. The $^4A_1$ and $^4E(^4G)$ have the same energy and are parallel to the ground level $^6A_1$. Therefore, the excitation band corresponding to $^6A_1$-$^4A_1$,$^4E(^4G)$ show a narrow band. The strong excitation band in 400-450 nm is consistent with the result of diffuse reflection spectra, showing good absorption in this wavelength range.

The emission spectra show a broad red emission band in the wavelength range of 550-800 nm peaked at 647 nm for the sample α-$LiZnBO_3$:xMn^{2+}(x=0.07). The peak position and the shape of the emission spectrum are independent from the excitation wavelength, which indicate that there is only one emission center in the phosphor and confirm that the activator ions (Mn^{2+}) occupy only one site position in α-$LiZnBO_3$ host lattice. The observed band is attributed to $^4T_1(^4G)$-$^6A_1(^6S)$ transition of Mn^{2+}. When excited at 431 nm, the FWHM of emission band is 80 nm, which is nearly the same as that of recently reported single Mn^{2+} doped red phosphor, such as CaZnOS:Eu^{2+} (60nm),[20] $KMgBO_3$:Mn^{2+} (70nm).[21] It can be observed that the emission band is

asymmetric. This phenomenon is caused mainly by efficiency energy transfer from the defect-related emission.[22,23]

As introduced above, there is only one crystallographic Zn site, which is tetrahedral coordination. Due to similar ionic radius and valence, Mn^{2+} is expected to occupy Zn^{2+}, thus yellow-green emission is anticipated, as is reported in $LiZnPO_4:Mn^{2+}$ [4] and $NaZnPO_4:Mn^{2+}$.[24] Because the d-d transitions of Mn^{2+} are spin and parity forbidden, the intensities of the emission peaks in the Mn^{2+} single doped phosphors are weak. In our study, however, strong red emission is observed, which is also reported in $CaZnOS:Mn^{2+}$ [6] and β-$Zn_3B_2O_6:Mn^{2+}$.[7] The strong intensities can be ascribed to a high absorption and a high quantum efficiency of Mn^{2+} in the host lattice, which is similar to that in the CaZnOS host.[6] According to the Tanabe-Sugano diagram, red emission of Mn^{2+} comes from a strong crystal field offered by host lattice. As crystal field increase, the transition energy between the $^4T_1$ and $^6A_1$ levels is predicted to decrease (shift to longer wavelengths).[25] Normally a strong crystal field results from (1) higher charged coordinating ions, as in oxy-nitrides; (2) shorter Mn-X distances in the host; and (3) level splitting.[6,7] For α-$LiZnBO_3$, Zn^{2+} is four-coordinated by O^{2-} and the average Zn-O distances is 1.972Å, which is very close to Zn-O distance in ZnO (1.977Å). Thus the first two reasons will not result in a strong crystal field in this study. Similar to the case in $CaZnOS:Mn^{2+}$,[6] β-$Zn_3B_2O_6:Mn^{2+}$,[7] and $Li_2ZnGeO_4:Mn^{2+}$,[15] Mn^{2+} occupies a distorted tetrahedral coordination site, resulting E and T levels of Mn^{2+} further splitting into more levels. Thus the first excited state (*i.e.* $^4T_1$) shift to lower energy and longer emission wavelength is observed.

Table 1 summarizes recent reported single Mn^{2+}-activated Zn-based phosphors with distorted tetrahedral coordination. These emit strong red color because of the abnormal luminescent property of Mn^{2+}. It can be seen that the average Zn-X distance are not proportional to the wavelength of the emission peak, which indicates that shorter Mn-X distances is not the prerequisite to result in the increase of the crystal field. This further deduces that the strong crystal field in this study should be from level splitting.

Effect of Lithium ventilation on emission intensity

Lithium ventilation during samples preparation at high temperature is a problem which results in the non-stoichiometry of the sample and therefore affects the emission properties. M. Pardha Saradhi at.al reported that lithium ion vacancies caused by ventilation can act as trapping centers which are responsible for the significant decrease in emission intensity.[26] In our study, however, lithium ventilation is found to have negligible influence on emission intensity, as is shown in Fig.6. PL intensity is almost the same when the lithium content is in the range from 0.9 to 1.05. This means α-$LiZnBO_3$:Mn^{2+} have a relatively high tolerance of compositional shift, which is very meaningful in the process of mass production. In addition, the decrease of the emission intensity with the increase of Li^+ concentration also confirms that Mn^{2+} will not occupy Li^+ site because the intensity of emission peak should increase if Li^+ is used as charge compensator.

Concentration quenching of Mn^{2+} in α-$LiZnBO_3$

Fig. 7(a) shows the emission spectra of α-$LiZnBO_3$:xMn^{2+} phosphors with Mn^{2+} concentration *x* varying from 0.05 to 0.11.When excited at 431nm, the peak position is located at 647 nm, regardless of Mn^{2+} concentration. The emission intensities increase

with increasing the doping concentration until reaching a maximum when x=0.07. Due to concentration quenching effect mainly caused by non-radiative energy migration among the identical activator Mn^{2+} ions, the emission intensities are found to decrease with the increasing of Mn^{2+} concentration, as shown in the inset of Fig. 7(b). The probability of energy transfer between two activators is inversely proportional to the n^{th} power of the distance between the activator ions. The distance between the Mn^{2+} ions becomes small as the concentration of Mn^{2+} increases. Therefore, the probability of energy migration increases.[27] The concentration quenching phenomena will not occur if the average distance between identical Mn^{2+} ions is so large that the energy migration is hampered. Thus the critical distance (R_c) is an important parameter which can be given by the following equation[28]

$$R_c \approx 2\left[\frac{3V}{4\pi x_c Z}\right]^{1/3} \quad (2)$$

where V is volume of the unit cell, x_c represents the quenching concentration and Z refers to the number of Mn^{2+} per unit cell. For α-$LiZnBO_3$:Mn^{2+}, V=239.26Å^3, x_c=0.07, Z=4, the calculated value of R_c is about 11.77 Å. The result indicates that the exchange interaction is not the main mechanism of energy transfer between Mn^{2+} in the α-$LiZnBO_3$ host because the critical distance for energy transfer in the mechanism of the exchange interaction is restricted to less than 5Å. The parity-forbidden d-d transition of Mn^{2+} in this study is extended somewhat because of the strong crystal field offered by distorted tetrahedral environment, the concentration quenching in the α-$LiZnBO_3$:Mn^{2+} should be

mainly controlled by an electric multipolar interaction process according to Dexter theory. The PL intensity (I) per activator is given by equation[29]

$$\frac{I}{x} = \frac{k}{1+\beta(x)^{\frac{\theta}{3}}} \quad (3)$$

where I is the emission intensity, x is the activator concentration; θ=6, 8, 10 correspond to dipole-dipole, dipole-quadrupole, and quadrupole-quadrupole interaction and k and β are constants for the given excitation condition and host crystal, respectively. When x exceeds critical concentration, equation 3 can be simplified as

$$\frac{I}{x} = \frac{k'}{\beta(x)^{\frac{\theta}{3}}} \quad (4)$$

As shown in Fig. 7(b), the value of θ is 7.8 as the slope=2.6. Since θ is very close to 8, the dipole-quadrupole interaction is responsible for concentration quenching observed in α-$LiZnBO_3$:Mn^{2+}.

Temperature-dependent PL of α-$LiZnBO_3$:Mn^{2+}

Fig. 8(a) shows the temperature-dependent PL spectra (λ_{ex}=431 nm) of α-$LiZnBO_3$:Mn^{2+} at the temperature range of 25 ^{o}C to 250 ^{o}C. The emission peaks at different temperature show similar shape with slight blue shift (Fig. 8(b)). As indicated by Arriortua et al.,[30] the blue shift of the emission band as the temperature increase is because of the thermal expansion of the host lattice with increasing temperature which results in a decrease of the crystal field and a concomitant increase in the emission energy of Mn^{2+}. The thermal quenching properties of α-$LiZnBO_3$:Mn^{2+} and commercial red

phosphor SrS:$Eu^{2+}$are compared in Fig. 8(c). As can be seen from Fig. 8(c), the thermal stability of α-$LiZnBO_3$:Mn^{2+} is superior to that of SrS:Eu^{2+}. Compared to the intensity of emission peak at room temperature, the integrated emission intensities at 75 °C and 125 °C remain about 79% and 64%. The results above show that this phosphor has a good thermal stability besides of the blue shift of the emission peak.

Generally, the luminescence thermal quenching effect is attributed to the non-radiative relaxation through the crossing point between the excited state and the ground state in the configurational coordinate diagram. As the temperature increases, the non-radiative transition probability by thermal activation increases, which decreases the luminescence. The decrease of the emission intensity of the phosphors depends on the temperature and can be described based on the following Arrhenius Equation [27,31]

$$I(\mathrm{T}) = \frac{I_0}{1 + c\exp(-\frac{E_a}{kT})} \quad (5)$$

where E_a is the activation energy, I_0 is the emission intensity at room temperature and I_T is the emission intensity at measuring temperatures, c is a constant, and k is Boltzmann constant (8.62×10^{-5}eV). Therefore, the activation energy E_a can be calculated from slope of the plot of $ln(I_0/I_T\text{-}1)$ vs $(1/kT)$. As is displayed in Fig. 8(d), E_a is determined to be 0.23 eV.

Quantum efficiency of α-$LiZnBO_3$:Mn^{2+}

The quantum efficiency of phosphor is an important parameter to be considered for practical application. To determine the absolute quantum efficiency of photo-conversion for the α-$LiZnBO_3$:0.07Mn^{2+} phosphor, the integrated sphere method is applied for the

measurements of optical absorbance (A) and quantum efficiency (η_{int}) of the phosphors. The absorbance can be calculated by using the following equation:

$$A = \frac{L_0(\lambda) - L_i(\lambda)}{L_0(\lambda)} \quad (6)$$

where $L_0(\lambda)$ is the integrated excitation profile when the sample is diffusely illuminated by the integrated sphere's surface, $L_i(\lambda)$ is the integrated excitation profile when the sample is directly excited by the incident beam. Furthermore, the internal quantum efficiency (η_{int}) of the phosphors can be calculated by

$$\eta_{int} = \frac{E_i(\lambda) - (1 - A)E_0(\lambda)}{L_e(\lambda)\,A} \quad (7)$$

where $E_i(\lambda)$ is the integrated luminescence of the powder upon direct excitation, and $E_0(\lambda)$ is the integrated luminescence of the powder excited by indirect illumination from the sphere. The term $L_e(\lambda)$ is the integrated excitation profile obtained from the empty integrated sphere (without the sample present). Upon excited at 431nm, the absorbance of α-$LiZnBO_3$:0.07Mn^{2+} is 71.5%, and the internal quantum efficiency (η_{int}) is found to be 44.2%. Thus, the external quantum efficiency η_{ext}=absorbance×η_{int}=31.6%, which is better than that of SrS:Eu^{2+} (absorbance=70.3%, η_{int}=31.3%, and η_{ext}=22.0%)[32].

Decay properties and chromaticity coordinate of α-$LiZnBO_3$:Mn^{2+}

Fig. 9 shows the decay curves of α-$LiZnBO_3$:Mn^{2+}(x=0.05, 0.06, 0.08, 0.09, 0.11). The decay curve can be fitted well by first-order exponential equation

$$I = I_0 \exp(-\frac{t}{\tau}) \quad (8)$$

where I_0 and I are the luminescence intensity at time 0 and t, τ is the lifetime of activator. Obviously, there is only one type of Mn^{2+} emission site in the host from the fitting results, which is in good agreement with the structural and PL studies. The luminescence decay lifetime is determined to be 5.57 ms, 5.39 ms, 5.25 ms, 5.11 ms, 4.83 ms, and 4.54 ms for α-$LiZnBO_3$:Mn^{2+} with x=0.05, 0.06, 0.08 0.09, 0.10, and 0.11. The results are consistent with the fact that the decay time of Mn^{2+} is usually in the millisecond range.[15,21] It can be seen that the decay time decrease with the increase of doping concentration, which is caused by super exchange interaction between Mn^{2+} pairs.

Fig.10 shows the Commission International de I'Eclairage (CIE1931) chromaticity coordinates at room temperature for α-$LiZnBO_3$:0.07 Mn^{2+} under the excitation wavelength of 431 nm. The chromaticity coordinate is calculated to be (0.66, 0.34), which is very close to standard red color (0.66, 0.33). It indicates the emission color of α-$LiZnBO_3$:Mn^{2+} is of high color purity and saturation.

Conclusion

In conclusion, we synthesized a red-emitting phosphor α-$LiZnBO_3$:Mn^{2+} by means of solid state reaction method. Mn^{2+} ions are expected to occupy Zn^{2+} site, which is 4-number coordinated. ESR spectra indicate that the doped ions are Mn^{2+}. The diffuse reflectance spectra and excitation spectra demonstrate that α-$LiZnBO_3$:Mn^{2+} can be excited at ~425 nm. Abnormal red emission from the transition of $^4T_1(^4G) \rightarrow {}^6A_1(^6S)$ was observed for tetrahedral coordinated Mn^{2+} in α-$LiZnBO_3$ due to a further splitting of Mn^{2+} level. The quenching concentration is 7 mol% and the critical distance is 11.77 Å. The chromaticity coordinate of the phosphor at room temperature is calculated to be (0.66,

0.34). Temperature-dependent PL spectra reveal that the synthesized phosphor is thermal stability, but the emission peak will move to the shorter wavelength as the temperature increase.

Acknowledgements

This work was financially supported by National Natural Science Foundation of China (51372121, 61274053, 90922037), Natural Science Foundation of Tianjin (14JCYBJC17800), and the Program for New Century Excellent Talents in University of China (NCET-11-0258).We thank Assoc. Prof. A. Yu in Nankai University and Prof. ZG Xia in University of Science and Technology Beijing for the ESR and temperature-dependent PL spectra measurement, respectively.

Notes and references

1. K.-S. Sohn, B. Cho and H. D. Park, *J. Am. Ceram. Soc.*, 1999, **82**, 2779.
2. T. Ohtake, N. Sonoyama and T. Sakata, *Electrochem. Comm.*, 2005, **7**, 1389.
3. X. Zhang, H. Zeng and Q. Su, *J. Alloys Compds.*, 2007, **441**, 259.
4. T.-S. Chan, R.-S. Liu and I. Baginskiy, *Chem. Mater.*, 2008, **20**, 1215.
5. G. Blasse and B. Grabmaier, *Luminescent materials*, Springer-Verlag Berlin, 1994.
6. C. J. Duan, A. C. A. Delsing and H. T. Hintzen, *Chem. Mater.*, 2009, **21**, 1010.
7. Y. Shi, Y. Wen, M. Que, G. Zhu and Y. Wang, *Dalton Trans*, 2014, **43**, 2418.
8. D. Chikte, S. K. Omanwar and S. V. Moharil, *J. Lumines.*, 2013, **142**, 180.
9. L. Tian, B.-Y. Yu, C.-H. Pyun, H. L. Park and S.-i. Mho, *Solid State Comm.*, 2004, **129**, 43.
10. L. Jia, Z. Shao, Q. Lü, Y. Tian and J. Han, *Opt. Laser Tech.*, 2013, **54**, 79.

11. X. Li, C. Liu, L. Guan, W. Wei, Z. Yang, Q. Guo and G. Fu, *Mater. Lett.*, 2012, **87**, 121.

12. J. Wang, S. Wang and Q. Su, *J. Mater. Chem.*, 2004, **14**, 2569.

13. H. A. Lehmann and H. Schadow, *Zeit. Anorg. Allg. Chem.*, 1966, **348**, 42.

14. X. Chen, C. Yang, X. Chang, H. Zang and W. Xiao, *Solid State Sci.*, 2009, **11**, 2086.

15. M. Shang, G. Li, D. Yang, X. Kang, C. Peng and J. Lin, *Dalton Trans.*, 2012, **41**, 8861.

16. R. Stefan, S. Simon, *Modern Phys. Lett. B*, 2001, **15**, 111.

17. J. W. H. Schreurs, *J. Chem. Phys.*, 1978, **69**, 1251.

18. N. Yamashita, *J. Phys. Soc. Jpn.*, 1973, **35**, 1089.

19. L. E. Orgel, *J. Chem. Phys.*, 1955, **23**, 1004.

20. T. W. Kuo, W. R. Liu, T. M. Chen, *Opt. Express,* 2010, **18**, 8187.

21. L. Wu, B. Wang, Y. Zhang, L. Li, H. R. Wang, H. Yi, Y. F. Kong, and J. J. Xu, *Dalton Trans.*, 2014, **43**, 13845.

22. K. S. Sohn, B. Cho, H. D. Park, *J. Am. Ceram. Soc.*, 1999, **82**, 2779.

23. Q. H. Zhang, J. Wang, C. W. Yeh, W. C. Ke, R. S. Liu, J. K. Tang, M. B. Xie, H. B. Liang, Q. Su, *Acta Mater.*, 2010, **58**, 6728.

24. D. Haranath, S. Mishra, S. Yadav, R. K. Sharma, L. M. Kandpal, N. Vijayan, M. K. Dalai, G. Sehgal and V. Shanker, *Appl. Phys. Lett*, 2012, **101**, 221905.

25. W. M. Yen and H. Yamamoto, *Phosphor handbook*, CRC press, 2012.

26. M. P. Saradhi and U. V. Varadaraju, *Chem. Mater.*, 2006, **18**, 5267.

27. H. Jing, C. Guo, G. Zhang, X. Su, Z. Yang and J. H. Jeong, *J. Mater. Chem.*, 2012, **22**, 13612.

28. G. Blasse, *Philips Res. Rep*, 1969, **24**, 131.

29. L. G. Van Uitert, *J. Electrochem. Soc.*, 1967, **114**, 1048.

30. J. Orive, R. Balda, J. Fernandez, L. Lezama and M. I. Arriortua, *Dalton Trans.*, 2013, **42**, 12481.

31. R.-J. Xie, N. Hirosaki, N. Kimura, K. Sakuma and M. Mitomo, *Appl. Phys. Lett.*, 2007, **90**, 191101.

32. Q. Xia, M. Batentschuk, A. Osvet, A. Winnacker and J. Schneider, *Radiat Meas*, 2010, **45**, 350.

Table 1. Characteristics of Mn^{2+} doped α-$LiZnBO_3$ phosphor as compared to those of typical Mn^{2+} doped Zn-based phosphors, in which the hosts afford tetrahedral crystal field environment and the phosphors emit red color at room temperature.

Phosphors	**β-$Zn_3B_2O_6$:Mn^{2+}**	**CaZnOS:Mn^{2+}**	**BaZnOS:Mn^{2+}**	**α-$LiZnBO_3$:Mn^{2+}**
Space group	*C2/c*	*$P6_3mc$*	*Cmcm*	*C2/c*
Body color	Yellow to earth yellow	White to pink	Light yellow to pink	White to pink
Mn^{2+}excitation bands (nm)	352, 377, 419, 432, 467	396, 438, 490	396, 438, 490	327, 356, 386, 422, 431, 453
Emission peak center (nm)	600	614	634	647
FWHM of emission bands (nm)	80	50	60	80
Average Zn-X distance (Å)	1.965	2.25	2.25	1.972
Ref.	7	6	6	this work

The abnormal red-emitting luminescent property of tetrahetral coordinated Mn^{2+} in α-$LiZnBO_3$ is observed.

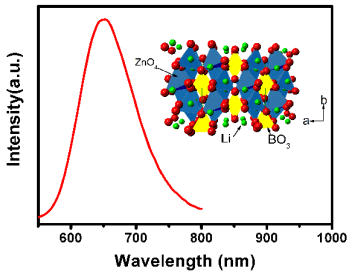

Figure Captions

Fig. 1 (a) The XRD patterns of α-$LiZnBO_3$:Mn^{2+} phosphors with different Mn^{2+} doping contents. (b) Crystal structure of α-$LiZnBO_3$ (along c axis).

Fig. 2 SEM morphology of α-$LiZnBO_3$:0.07Mn^{2+} phosphor.

Fig. 3 X-band powdered ESR spectra at room temperature of α-$LiZnBO_3$:xMn^{2+} (x=0.001, 0.01, 0.02, 0.04) sample. Inset is the case of α-$LiZnBO_3$:0.001Mn^{2+}.

Fig. 4 Diffuse reflection spectra of α-$LiZnBO_3$:xMn^{2+} sample. Inset shows the absorption spectrum (K/S) of α-$LiZnBO_3$ and α-$LiZnBO_3$:0.07Mn^{2+} derived with the Kubelka-Munk function.

Fig. 5 Typical excitation spectra monitored at 647 nm and emission spectra excited at different wavelength of α-$LiZnBO_3$:0.07Mn^{2+} at room temperature.

Fig. 6 PL spectra of α-Li_xZnBO_3:0.07Mn^{2+} with different lithium content (x=0.8, 0.9, 1, 1.05, 1.1, 1.2). Inset is the plot of intensity of emission peak *vs*. content of Li^+.

Fig. 7 (a) Excitation and emission spectra of α-$LiZnBO_3$:*x*Mn^{2+} phosphors with different Mn^{2+} doping concentrations. (b) Dependence of lg(*I*/*x*) on lg*x*, where I is the emission intensity and *x* is the concentration of Mn^{2+}. Inset is the emission intensity *vs.* Mn^{2+} concentration (*x*) of α-$LiZnBO_3$:*x*Mn^{2+} phosphor.

Fig. 8 (a) Temperature-dependent PL spectra of α-$LiZnBO_3$:0.07Mn^{2+} phosphor (λ_{ex}=431 nm). (b) Dependence of wavelength of emission peak on the temperature. (c) Normalized PL intensity as a function of temperature. As a comparison, thermal quenching data of SrS:Eu^{2+}excited at 460 nm are also measured as a reference. (d) the ln (I_0/I_T-1) *vs*. $1/k_BT$ activation energy graph for thermal quenching of α-$LiZnBO_3$:0.07Mn^{2+}.

Fig. 9 Room temperature decay curves ofα-$LiZnBO_3$:xMn^{2+} with Mn^{2+} contents (x=0.05, 0.06, 0.08, 0.09, 0.10, 0.11) (excited at 431 nm, monitored at 647 nm).

Fig. 10 CIE chromaticity diagram forα-$LiZnBO_3$:0.07Mn^{2+} excited at 431 nm.

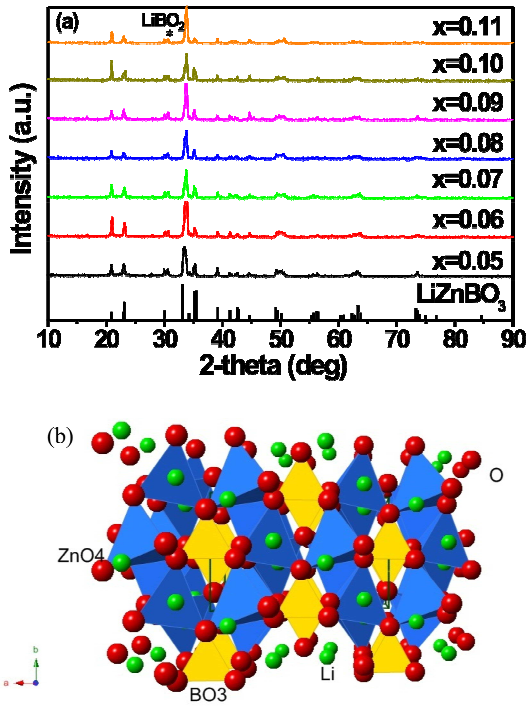

Fig. 1 (a) The XRD patterns of α-$LiZnBO_3$:Mn^{2+} phosphors with different Mn^{2+} doping contents. (b) Crystal structure of α-$LiZnBO_3$ (along c axis).

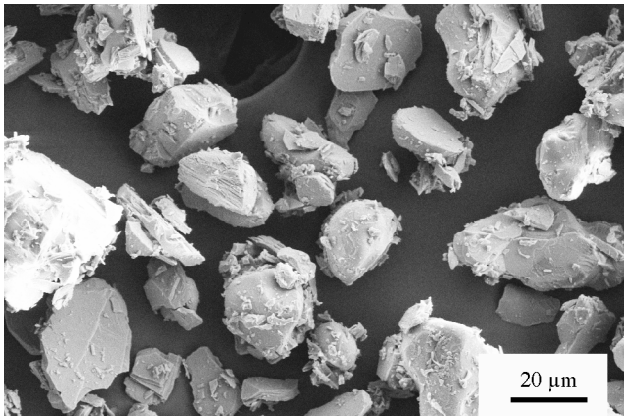

Fig. 2 SEM morphology of α-$LiZnBO_3$:0.07Mn^{2+} phosphor.

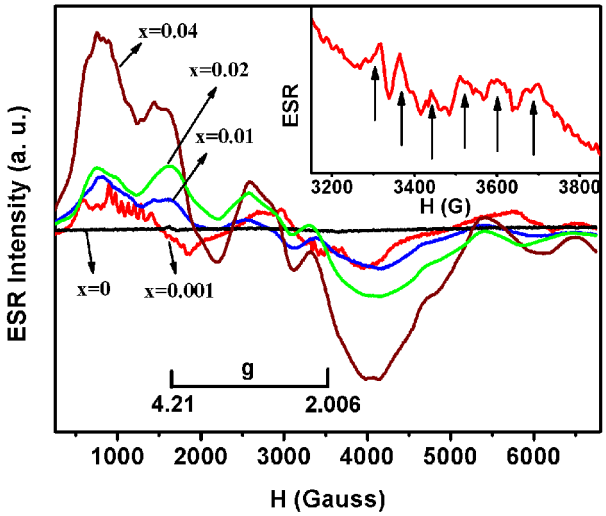

Fig. 3 X-band powdered ESR spectra at room temperature of α-$LiZnBO_3$:xMn^{2+} (x=0, 0.001, 0.01, 0.02, 0.04) samples. Inset is the case of α-$LiZnBO_3$:0.001Mn^{2+}.

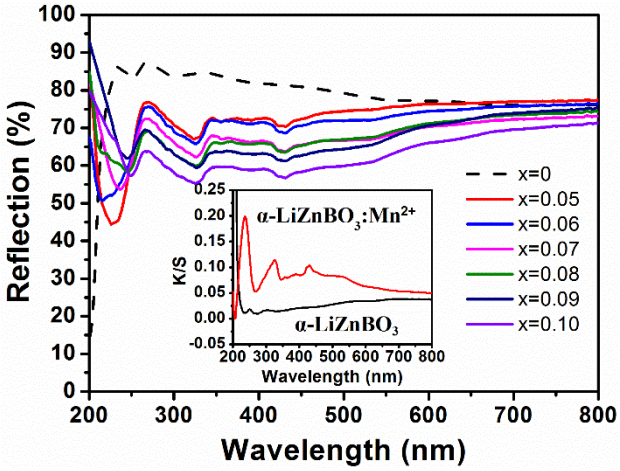

Fig. 4 Diffuse reflection spectra of α-$LiZnBO_3$:xMn^{2+} sample. Inset shows the absorption spectrum (K/S) of α-$LiZnBO_3$ and α-$LiZnBO_3$:0.07Mn^{2+} derived with the Kubelka-Munk function.

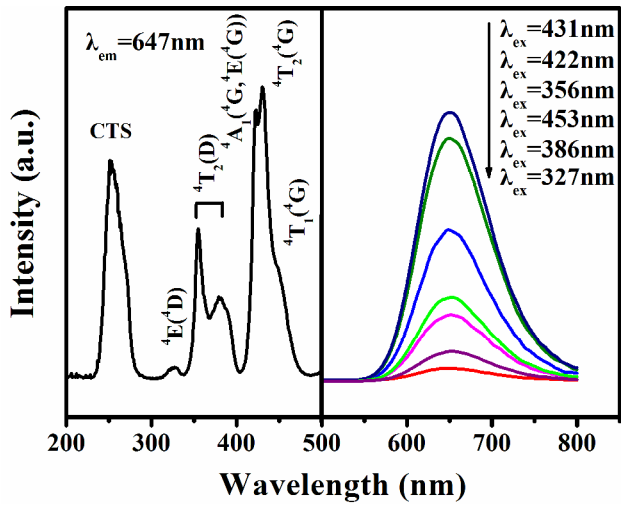

Fig. 5 Typical excitation spectra monitored at 647 nm and emission spectra excited at different wavelength of α-$LiZnBO_3$:0.07Mn^{2+} at room temperature.

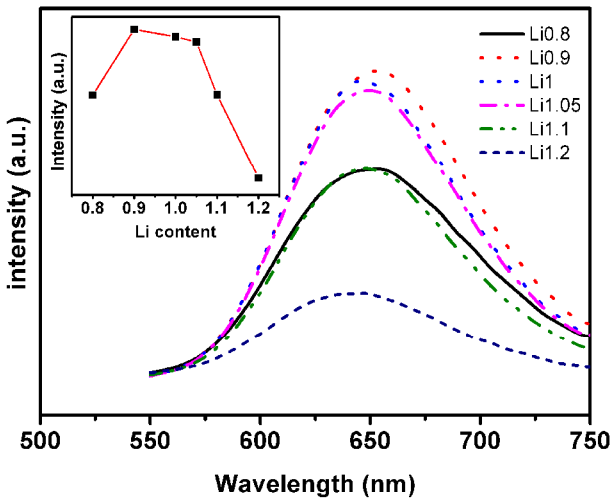

Fig. 6 PL spectra of α-Li_xZnBO_3:0.07Mn^{2+} with different lithium content (x=0.8, 0.9, 1, 1.05, 1.1, 1.2). Inset is the plot of intensity of emission peak *vs*. content of Li^+.

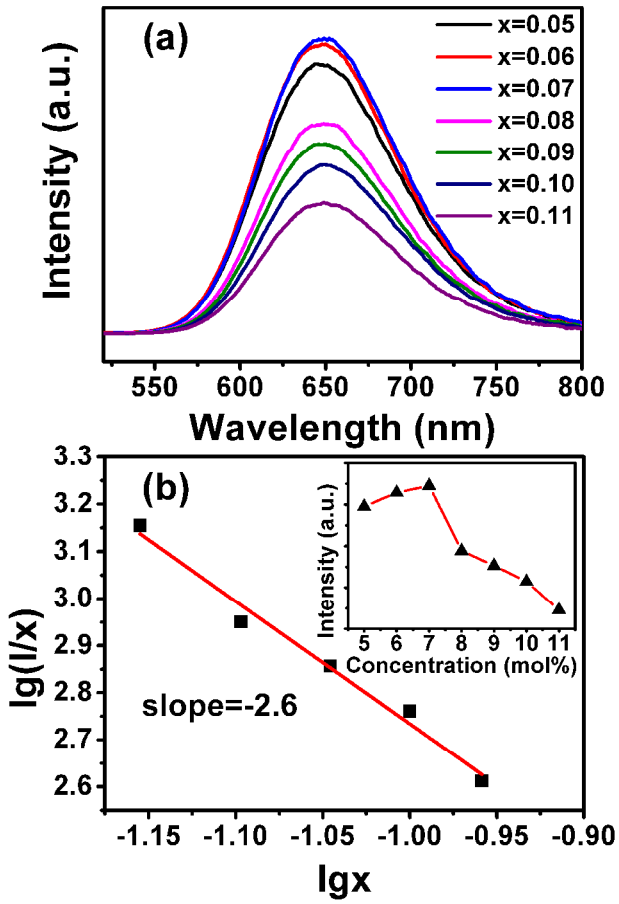

Fig. 7 (a) Excitation and emission spectra of α-$LiZnBO_3$:$x$$Mn^{2+}$ phosphors with different Mn^{2+} doping concentrations. (b) Dependence of lg(I/x) on lg$x$, where I is the emission intensity and x is the concentration of Mn^{2+}. Inset is the emission intensity *vs.* Mn^{2+} concentration (x) of α-$LiZnBO_3$:$x$$Mn^{2+}$ phosphor.

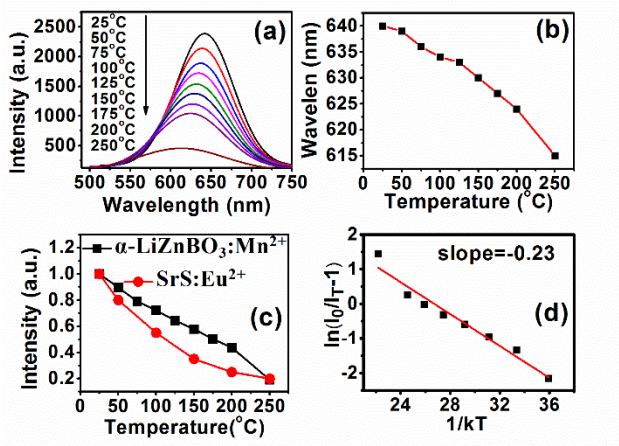

Fig. 8 (a) Temperature-dependent PL spectra of α-$LiZnBO_3$:0.07Mn^{2+} phosphor (λ_{ex}=431 nm). (b) Dependence of wavelength of emission peak on the temperature. (c) Normalized PL intensity as a function of temperature. As a comparison, thermal quenching data of SrS:Eu^{2+}excited at 460 nm are also measured as a reference. (d) the ln (I_0/I_T-1) *vs*. 1/k_BT activation energy graph for thermal quenching of α-$LiZnBO_3$:0.07Mn^{2+}.

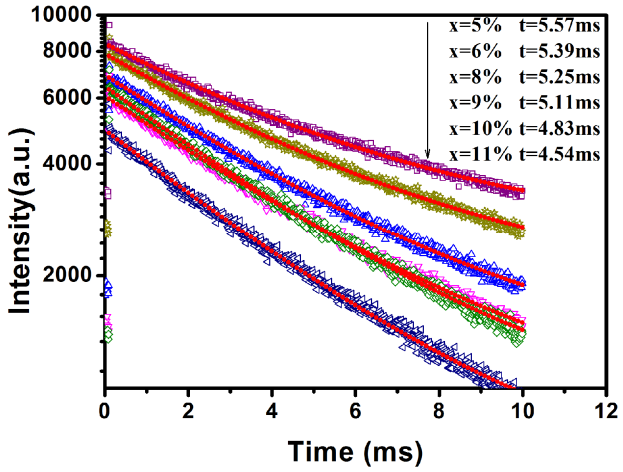

Fig. 9 Room temperature decay curves ofα-$LiZnBO_3$:xMn^{2+} with Mn^{2+} contents (x=0.05, 0.06, 0.08, 0.09, 0.10, 0.11) (excited at 431 nm, monitored at 647 nm).

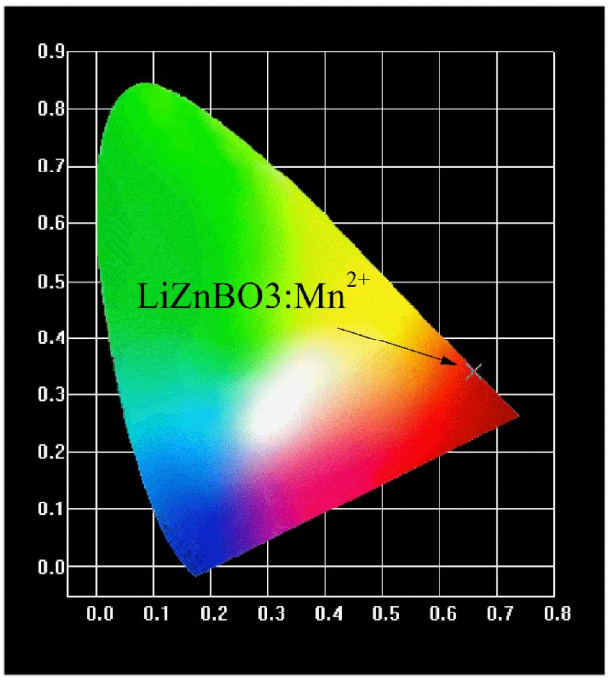

Fig. 10 CIE chromaticity diagram forα-$LiZnBO_3$:0.07Mn^{2+} excited at 431 nm.